Geochemistry, Geophysics, Geosystems

RESEARCH ARTICLE
10.1029/2020GC009360

Changing Brine Inputs Into Hydrothermal Fluids: Southern Cleft Segment, Juan de Fuca Ridge

C. Geoffrey Wheat[1], Robert A. Zierenberg[2], Jennifer B. Paduan[3], David W. Caress[3], David A. Clague[3], and William W. Chadwick Jr.[4]

[1]Institute of Marine Sciences, College of Fisheries and Ocean Sciences, University of Alaska Fairbanks, Moss Landing, CA, USA, [2]Department of Earth and Planetary Sciences, University of California Davis, Davis, CA, USA, [3]Monterey Bay Aquarium Research Institute, Moss Landing, CA, USA, [4]Cooperative Institute for Marine Resources Studies (CIMRS), Hatfield Marine Science Center, Oregon State University, Newport, OR, USA

Key Points:

- Thermal and chemical data provide a 32-year record of brine-dominated hydrothermal discharge from the Cleft Segment, Juan de Fuca Ridge
- The brine component is a deep-sourced (>2 km below the seafloor), hot (>400°C) fluid that mixes with hydrothermal fluid before discharge
- Compilation of mid-ocean ridge endmember compositions with >700 mmol Cl/kg shows uniform trends, implying brine composition is globally consistent

Supporting Information:

- Supporting Information S1
- Supporting Information S2

Correspondence to:
C. G. Wheat,
wheat@mbari.org

Citation:
Wheat, C. G., Zierenberg, R. A., Paduan, J. B., Caress, D. W., Clague, D. A., & Chadwick Jr., W. W. (2020). Changing brine inputs into hydrothermal fluids: Southern Cleft Segment, Juan de Fuca Ridge. *Geochemistry, Geophysics, Geosystems*, *21*, e2020GC009360. https://doi.org/10.1029/2020GC009360

Received 6 AUG 2020
Accepted 21 SEP 2020

Abstract In 2016, temperature recorders were recovered, temperatures were measured, and fluid samples were collected from Vent 1, a high temperature (338°C) hydrothermal discharge site on the southern Cleft Segment of the Juan de Fuca Ridge. Coupled with previous sampling efforts, this collection represents a 32-year record of discharge from a single chimney structure, the longest record to date. Remarkably, the fluid has remained brine-dominated for more than three decades. This brine formed during phase separation and segregation prior to initial observations in 1984. Although the chloride concentration of the discharging fluid has decreased with time, the fluid temperature has remained nearly constant for at least 3.3 years and probably for 15 or even 22 years. Compositions of the discharging fluids are consistent with inputs from a deep-sourced brine, which was last equilibrated at >400°C at a depth consistent with the base of the sheeted dikes and the brittle-ductile transition. This brine mixed (diffusion or dispersion) with a likely non-phase-separated, hydrothermal fluid prior to discharge. A survey of hydrothermal endmember fluids with chlorinities in excess of 700 mmol/kg shows, with the exception of Fe, a single trend between major ion concentrations and chlorinity even though data are from a range of crustal compositions, spreading rates, and water and magma depths. Calculated deep-sourced brines from hydrothermal fluid data are similar to data based on fluid inclusions and estimates of brine assimilation in magmas. A better understanding of brines is required given their potential duration of discharge and capacity for mobilizing metals.

Plain Language Summary Magma from the mantle ascends forming new oceanic crust that is cooled by hydrothermal processes. Seawater within the permeable crust is heated and reacts with rock before discharging at the seafloor, forming high temperature (>300°C) hydrothermal fluids and metal-rich deposits. In some cases, circulating seawater is heated to form vapor-and brine-dominated phases. The latter, because of its greater density, largely remains within the crust, resulting in a segregation of the two phases. This study focuses on a brine-dominated hydrothermal system on the Juan de Fuca Ridge (northeastern Pacific Ocean) that has remained relatively uniform for 32 years. During this period, the amount of brine input to a likely non-phase-separated hydrothermal fluid has decreased while the temperature (338°C) has remained constant, possibly for the past 15–22 years. We propose that the brine resides at depth and is incorporated into the circulating hydrothermal fluid. We use new data and a compilation of data from many different seafloor hydrothermal systems to constrain the compositions of circulating hydrothermal fluid and brine, which is globally consistent. Brine-dominated hydrothermal systems have been largely overlooked, but are capable of mobilizing metals from new oceanic crust and can persist for decades or longer.

1. Introduction

New oceanic crust forms with the intrusion of magma, which is cooled by seawater and drives convective circulation beneath the seafloor. Such circulation allows for the exchange of heat and elements prior to discharging hydrothermal fluids at the seafloor. These hydrothermal fluids impact ocean biogeochemistry and support primary production for one of the Earth's biomes (e.g., Humphris & Klein, 2018; Mullineaux et al., 2018). This circulation is not constant but responds to episodic magmatic intrusions, leading to periods of extensive seawater discharge immediately after a magmatic event followed by a much longer

period of sustained hydrothermal discharge (Baker et al., 1995, 1987; D'Asaro et al., 1994; Lowell & Germanovich, 1995). Furthermore, intruded magma provides a thermal boundary (~1,200°C) at depth, and depending on the path of fluid circulation, circulating seawater can be heated sufficiently to result in phase separation, forming coexisting vapor and brine (or liquid) phases (Bischoff & Rosenbauer, 1987; Delaney et al., 1987; Von Damm & Bischoff, 1987). Segregation of these two phases has been observed on a range of scales from a single structure (Von Damm et al., 2003) to adjacent structures (Massoth et al., 1989) and ridge segments (Butterfield & Massoth, 1994).

Butterfield et al. (1997) modeled the physical and chemical evolution in hydrothermal systems after a magmatic intrusion, predicting the discharge of a short-lived, gas-rich vapor phase followed by a longer-lived phase influenced by brines. The latter, because of its greater density, may accumulate at the depth of diabase dikes and gabbros near the brittle-ductile transition. This brine is potentially released to the overlying circulating seawater when the heat flux wanes or during magmatic eruptions at the seafloor (e.g., Bischoff & Rosenbauer, 1987; Coumou et al., 2009; Xu et al., 2018). Another model suggests that the brine resides in numerous minimally connected pore spaces within the basaltic matrix, particularly between pillow and sheet flows where there is a significant change in crustal permeability (Fontaine & Wilcock, 2006). The extent to which fluid segregation impacts the mobilization of metals is unspecified; however, relative to non-phase-separated hydrothermal discharge, it affects the partitioning of acid-generating volatile components in vapor phases (Lilley et al., 2003; Seewald et al., 2003) and creates high-chloride brines with increased potential for mobilizing metals as metal-chloride complexes (Bischoff & Rosenbauer, 1987; Foustoukos & Seyfried, 2007; Pester et al., 2015). Thus, biogeochemical and metal fluxes from hydrothermal systems depend on the partitioning of vapor-dominated, brine-dominated, and "stable" discharge. We define stable discharge as a non-phase-separated, Mg- and sulfate-depleted hydrothermal fluid that has undergone exchange with igneous crust at temperatures in excess of 300°C.

The extent of phase separation and segregation versus stable discharge is highlighted in several multiyear collections of hydrothermal fluids. Most multiyear studies have focused on active magmatic environments, which, consistent with Butterfield's et al. (1997) model, would be dominated by vapor-rich fluids. Examples include the 17-year-long study of hydrothermal systems from 9 to 10°N on the East Pacific Rise (EPR; Fornari et al., 2012; Pester et al., 2014; Von Damm, 2004) and discharge from the Main Endeavor Field on the Juan de Fuca Ridge (JFR), which actively discharged a vapor-dominated fluid for 15 years prior to a 1999 magmatic event (Butterfield et al., 1994; Lilley et al., 2003; Seyfried et al., 2003). In contrast, brine-dominated fluids with chlorinities in excess of 700 mmol/kg, well above the chlorinity of bottom seawater (~540 mmol/kg), are rare among the ~500 sampled hydrothermal sites globally (Humphris & Klein, 2018), thus little is known about long-term compositional changes of brine-dominated fluids, which can potentially discharge for centuries or longer (e.g., Choi & Lowell, 2015; Coumou et al., 2009; Han et al., 2013; Scott et al., 2016).

Some of the highest chlorinities ever recorded were measured in fluids collected from the northern Cleft (Butterfield & Massoth, 1994) and southern Cleft Segments (Trefry et al., 1994; Von Damm & Bischoff, 1987) of the JFR. Here chlorinities reached twice the seawater concentration. On the northern Cleft Segment, fluids depleted in chlorinity relative to seawater were collected in 1988, shortly after a documented eruption, probably in 1986 (Baker et al., 1987; Chadwick et al., 1991; Embley et al., 1991; Fox et al., 1992). Two years later in 1990, fluids with chlorinities in excess of seawater were collected (Butterfield & Massoth, 1994). Subsequent fluid samples collected over the following 2 years were progressively dilute (Butterfield & Massoth, 1994). In contrast, only high chlorinity hydrothermal fluids have been collected from the southern Cleft Segment, with values as high as 1,140 mmol/kg (Von Damm & Bischoff, 1987). No known eruption has occurred on southern Cleft Segment since the earliest seafloor studies in the early 1980s (Normark et al., 1983, 1986), where light sediment cover on extensive flows suggests that the last eruption on this segment may date back centuries.

In 2016, we collected hydrothermal fluid samples, made thermal measurements of discharging fluids, and recovered a high-temperature HOBO probe from Vent 1 on the southern Cleft Segment (Figure 1). This discharge site was first sampled in 1984 (Von Damm & Bischoff, 1987) and sampled again in 1990, 1991, and 1994 (Metz & Trefry, 2000; Trefry et al., 1994) and 2016 (this work), resulting in a 32-year time series of fluid composition. This site was also instrumented with temperature probes intermittently during this

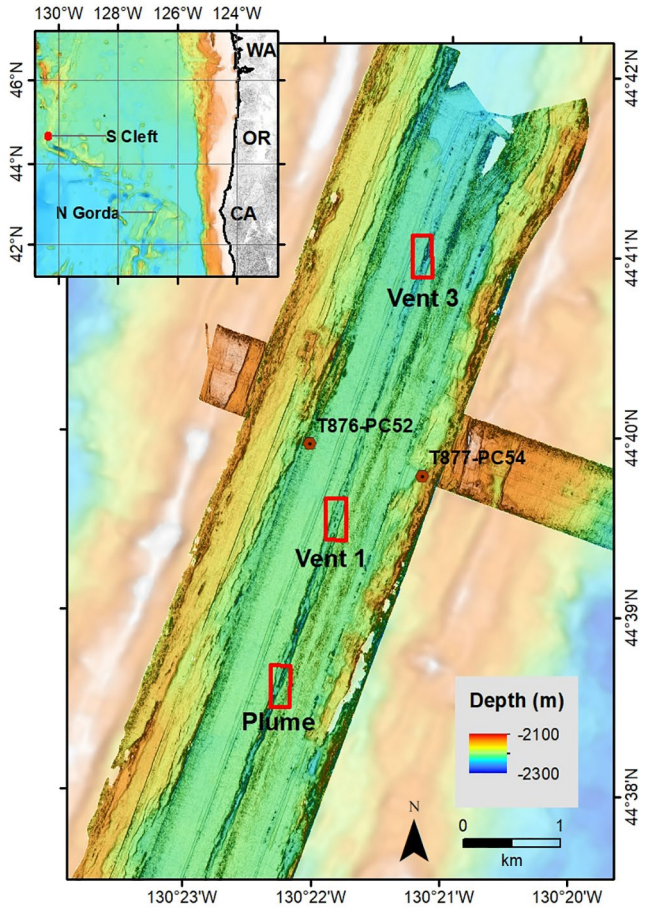

Figure 1. Map of the southern Cleft Segment of the Juan de Fuca Ridge located in the northeastern Pacific Ocean off the coast of Oregon, USA. Three portions of the southern Cleft Segment are known to support active hydrothermal discharge (Plume, Vent 1, and Vent 3). More detailed bathymetric maps of the three areas defined by the red boxes are provided in Figures S5 and S6. Map shows DSL-120 bathymetry at 2-m resolution, over more-faded EM300 bathymetry at 20-m resolution (Monterey Bay Aquarium Research Institute [MBARI] Mapping Team, 2001). Locations of two of three sediment cores that were used to date depositional rates (Table S9) are labeled.

32-year period. Data show a monotonic decrease in chlorinity while the temperature remained generally stable at ~338°C. We use this thermal and chemical record of discharging fluids to predict exchange and reaction processes within the crust that constrain models for hydrothermal convection and to evaluate the stage of the southern Cleft Segment within the context of Butterfield's et al. (1997) model. In addition, we provide new sediment data that constrain estimates for the timing of the latest eruption on the southern Cleft Segment, providing a context for the longevity of a potential brine-influenced discharge. With these new data and those from prior sampling of the southern Cleft Segment, we also evaluate the chemical composition of the brine and compare it to findings from fluid inclusions that were recovered by drilling into an active hydrothermal reaction zone in the sheeted dike complex underlying the Reykjanes Geothermal Field, Iceland (Bali et al., 2020) and estimates of brine assimilation in magma (e.g., Coombs et al., 2004; Kent et al., 1999; Magenheim et al., 1995; Michael & Cornell, 1998). Together, these data provide the longest time series of any oceanic hydrothermal discharge site, provide a measure of the composition of a consistent stable hydrothermal fluid and deep-sourced brine, and place constraints for future experiments and modeling simulations to better understand hydrologic processes, water-rock reactions, metal mobilization within high-temperature hydrothermal reaction zones, and integrated fluxes from non-phase-separated-, vapor-, and brine-dominated discharge.

2. Geologic Setting and Methods

The southern Cleft segment of the JFR is a medium-spreading rate (full-spreading rate 4.95 cm/year; DeMets et al., 2010), broad, flat ridge with a shallow, symmetric axial graben that is 1-km wide and 100-m deep (Normark et al., 1986; Figure 1). Early SeaBeam and SeaMARC II mapping (Embley & Chadwick, 1994; Normark et al., 1986) were followed in 1998 with an EM300 multibeam sonar system (Monterey Bay Aquarium Research Institute [MBARI] Mapping Team, 2001) that generated bathymetry of the Cleft Segment with ~20-m horizontal resolution. Also in 1998, two higher-resolution systems were used to map the axial valley of the southern Cleft Segment. The first was a DSL-120 side scan sonar, which was towed from the ship at about 100 m off the seafloor (Expedition TN082, DSL-120 dive 050; Stakes et al., 1998). This is the first publication of these data, which have a horizontal resolution of 2 m (Figures S1–S3). This system produced backscatter data (Figure S1a), which were obtained from the amplitude of the signal, and bathymetry (Figure S1b) data, which were calculated based on the phase difference of the signal returning to paired transducers (Scheirer et al., 2000). The second system and one also employed in 1998–1999, was an Imagenex "pencil-beam" scanning sonar that transmitted a narrow pulse at 675 kHz to collect soundings for high-resolution bathymetry (Figures S3 and S4). This system was mounted to the remotely operated vehicle (ROV) *Jason* (dives J236 and J265–J268) and flew at an altitude of 25 m. The resulting map has a vertical resolution of less than 1 m and lateral resolution of 2–5 m, which is a function of data density (Chadwick et al., 2001).

The smooth, flat axial valley was covered by a young (decades to centuries before 1980), glassy, lobate ferrobasalt (normal mid-ocean ridge [MOR] basalt) sheet flow (Eaby et al., 1984) that erupted from a central fissure tens of meters wide, at least 10-km long and 5–20-m deep (Normark et al., 1986), giving rise to the name Cleft Segment. This eruption may have been centered on the Plume area, a site of active hydrothermal discharge that was first explored using the submersible *Alvin* in September 1984 (Normark et al., 1986), although Chadwick et al., 2001), based on the higher resolution Imagenex data, did not support that

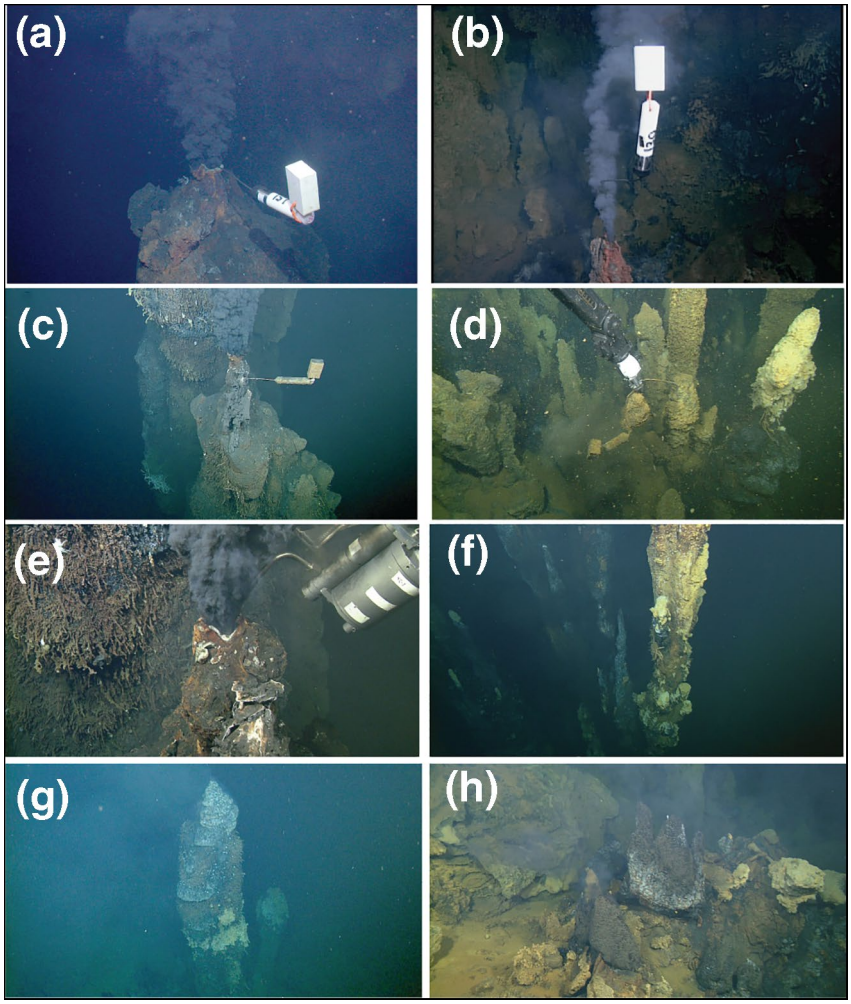

Figure 2. Images of remotely operated vehicle (ROV) framegrabs from 2005 (ROV *Tiburon,* T876) and 2016 (ROV *Doc Ricketts,* D875). (a) HOBO151 temperature probe is shown after deployment at Vent 1 in 2005. (b) HOBO130 temperature probe is shown after deployment at Plume in 2005. (c) HOBO151 is shown prior to recovery at Vent 1 in 2016. (d) HOBO130 is shown during recovery at Plume in 2016. (e) One of four Walden-Weiss titanium fluid samplers collects a sample from Vent 1 in 2016. (f) Hydrothermal spires are up to ~10 m in height at Vent 1 in 2016. (g) Hydrothermally active chimneys were located 300 m NNE of Plume, 2016. (h) Hydrothermal fluids discharge from deposits on the wall of the fissure at the site located 300 m NNE of Plume, 2016. Locations for each of these images are shown in Figure S6.

interpretation. Three areas of active high-temperature fluid discharge (Plume, Vent 1, and Vent 3) were discovered and sampled, each located along the walls of the central cleft fissure (Normark et al., 1986; Von Damm & Bischoff, 1987; e.g., Figure 2). Another four hydrothermal discharge sites were discovered, but not sampled (Normark et al., 1987; e.g., Figures 2g and 2h).

The maximum temperatures measured in 1984 were 285°C at Vent 1 and 224°C at the Plume site, but temperatures could not be measured for some samples (Von Damm et al., 1985). Metz and Trefry (2000) reported a temperature of 246°C for the Plume site, and temperatures of 332°C, 332°C, and 342°C at Vent 1 in 1990, 1991, and 1994, respectively. Continuous temperature data were recorded every 30 min or 1 h from three high-temperature HOBO probes that were recovered from the Plume site (recording from September 1999 to July 2001, July 2001 to October 2004, and August 2005 to April 2006), and four from the Vent 1 site (recording from September 1999 to July 2000, July 2001 to May 2004 [2 probes], and August 2005 to October 2008; Tables S1–S7 and Figures 2a and 2b; Chadwick, 2016). Dziak et al. (2003) reported temperature changes for two of these records associated with an earthquake on the Blanco Fracture Zone in 2000. Additional

HOBO probes were deployed in August 2005 on MBARI ROV *Tiburon* dives, but when MBARI returned in July 2016 only one HOBO probe from each of Plume and Vent 1 sites was recovered on ROV *Doc Ricketts* dives D874 and D875 (Figures 2c and 2d). These and temperature measurements that were made while sampling fluids from the Vent 1 site are discussed below.

Discharging fluids were collected in Walden-Weiss titanium major-element fluid samplers in 1984 (Von Damm et al., 1985) and during three expeditions conducted from September 1990 through June 1994 (Metz & Trefry, 2000). Four samples were collected in Walden-Weiss samplers from Vent 1 during the ROV *Doc Ricketts* dive D875 in 2016 (Figure 2e), providing an intermittent 32-year record of compositional changes in discharging fluids from the Vent 1 site. Sampling and analytical procedures for the four samples collected in 2016 were generally similar to those employed in previous studies. An additional sample of bottom seawater was collected in a Niskin bottle mounted on the ROV. This sample was collected ~200 m above the seafloor (1950 m) away from ascending hydrothermal fluids. For all five samples, fluids were extracted upon recovery and stored in high-density polyethylene bottles that were soaked for 24 h at 60°C in 10% HCl prior to rinsing with purified (18 MΩ cm) water. One milliliter was immediately removed and diluted in 19 ml of 10% HCl. Another aliquot was filtered. Chlorinity was measured ashore via titration with silver nitrate with a precision of ~0.2% on the filtered aliquot. The remainder of the data were determined from analyzing fluid from the 1:20 dilution and filtered aliquots via inductively coupled plasma-optical emission spectrometry with a precision of ~2% (Table S8).

Sediment accumulation rates were determined for three push cores that were collected on MBARI ROV *Tiburon* dives T876 and T877 in 2005 (Figure 1) and T460 in 2002 (Figure S1) to improve estimates for the age of the last lava flows that erupted from the southern Cleft Segment, and therefore determine the maximum age of the hydrothermal system. The cores were extruded in stratigraphic slices. Foraminifera were sieved from the refrigerated core intervals and ^{14}C ages obtained using methods described in Clague et al. (2013). The length of the cores and estimated basal ages were combined to determine the average regional sediment accumulation rate, which was then combined with estimates of sediment thickness on basaltic flows to estimate the age of the flow. Core ages were calibrated to calendar years (Table S9).

Two sulfide chimney samples were recovered from the chimneys from which the two HOBOs were recovered in 2016. In both cases, the HOBO was entombed in the sulfide chimney. Analyses of chimney fragments D875-R1 and -R2 are reported in Table S10 using the methods of Paduan et al. (2018).

3. Results

The high-resolution bathymetric surveys that mapped discharge sites on the southern portion of the Cleft Segment are shown in Figure 1. The DSL-120 survey was 2-km wide and covered the entire axial valley (Figures S1–S3). This survey was 22 km along-axis from the known discharge sites south to the intersection with the Blanco Transform. This survey also included a 6.5-km-long crossing line on the eastern flank of the ridge segment (Stakes et al., 1998; Figures S1–S3). Imagenex surveys covered a length of 6.4 km in the central fissure (the Cleft) over Plume and Vent 1 (but was offset at Vent 3) and some of the axial valley floor (Chadwick et al., 2001;Figures S3 and S4). Both surveys suggest elevated topography at Vent 1 and Plume (Figures S5a and S5b), and the DSL-120 bathymetry suggests elevated topography near Vent 3, 50–100 m from the United States Geological Survey position for the hydrothermal discharge site (Figure S5c). The resolution of these surveys is not adequate to resolve the narrow spires of individual chimneys (e.g., Figures 2d, 2f, and S6) in contrast to newer autonomous underwater vehicle-mounted bathymetric systems (Clague et al., 2020; Paduan et al., 2018).

Temperatures were measured using point measurements from undersea vehicles and from continuous records of high-temperature HOBO probes (Figure 3a). At Vent 1, the sulfide chimney (D875-R1 on Figure S5a) in which the recovered temperature recorder (HOBO151) was deployed in 2005, had sealed and overgrown the probe tip by 2016 (Figure 2c). Recovered chimney fragments were copper-rich, similar to material collected from this site in 1984 (Normark et al., 1986), and were enriched in Co, In, and Se (Table S10). Measured temperatures at this site varied by less than 10°C (332°C–342°C) from 1990 to 2016 (Figure 3a). This included two continuous recording periods from the same structure (July 2001 to May 2004 and August 2005 to October 2008). The former consisted of two probe deployments with average temperatures of 329°C

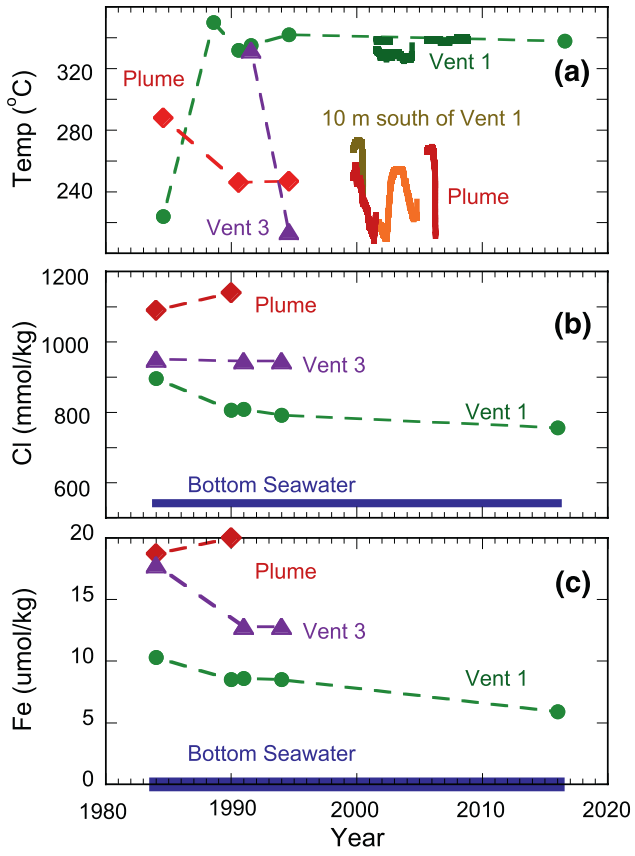

Figure 3. Temperature and concentrations of solutes (chlorinity and Fe) of discharging fluids from 1984 to 2016 at Plume, Vent 1, and Vent 3 hydrothermal sites on the southern Cleft Segment of the Juan de Fuca Ridge. Temperature data included discrete measurements (connected by dashed lines) using a submersible or remotely operated vehicle and seven deployments of temperature sensors that recorded temperatures at periods of 30 min–1 h (Tables S1–S7). Two temperature recorders were deployed in 2001 at Vent 1. Continuous temperature records from Plume decrease after a period of time as the chimney structure builds. Two shades of red/orange were used to highlight different probes deployed at the Plume site. Bottom seawater (blue) concentrations are shown for reference. Data are from Von Damm and Bischoff (1987), Trefry et al. (1994), Metz and Trefry (2000), and this work (Table 1 and Tables S1–S7).

± 1°C and 338°C ± 1°C, respectively, and the latter consisted of one probe deployment, the one recovered in 2016, that measured an average temperature of 339°C ± 1°C with a range of 3.6°C, which is about twice the precision afforded by the instrument. The cooler recorded temperature from the deployment in 2001 was positioned in a different structure about 10 m from the primary chimney, which could be naturally cooler. Alternatively, the lower temperature may have resulted from the difficulty in positioning the probe tip into the most intense flow. An additional issue is postemplacement chimney growth and exclusion of the tip from the primary source of discharge. For example, the continuous temperature records from the Plume site decrease after a period of time to temperatures below the recording range. HOBO130 was entombed within a Zn-rich sulfide chimney that was similar to those collected from the Plume site in 1984 (Normark et al., 1986). The 2016 recovered chimney sample was enriched in trace elements that are typically associated with sphalerite-rich samples, including Ag, As, Cd, Ge, Pb, and Hg (Table S10).

In 2016, we also used the high-temperature probe on the ROV *Doc Ricketts* and measured a maximum temperature of 338°C in Vent 1 (Figure 3a). This measurement was taken from an active orifice within tens of centimeters of where the embedded HOBO151 temperature probe was deployed (Figure 2c). Fluid samples were collected from this orifice (Figure 2e).

Bottom seawater is often entrained during the collection of hydrothermal fluids that discharge from a small edifice. A measure of the extent of entrainment is the concentration of dissolved Mg in collected fluids. Magnesium is presumed to be depleted in the high-temperature endmember. Measured Mg concentrations in the four hydrothermal fluids collected from Vent 1 in 2016 ranged from 1 to 2.4 mmol/kg (Table S8), which represents a maximum of 2%–4.5% dilution with bottom seawater. Given this minimal level of entrainment, endmember concentrations were calculated by extrapolating to a depleted Mg (0 mml/kg) fluid using the hydrothermal and bottom seawater data (Table 1).

This endmember composition was plotted with previous data to assess if there was a systematic variation in the hydrothermal fluid composition that discharged from Vent 1 over a 32-year period, from 1984 to 2016 (Figure 3). Chlorinity, for example, decreased from 896 mmol/kg in 1984 to 818 mmol/kg in 1990 to 792 mmol/kg in 1994 to 756 mmol/kg in 2016 (Figure 3b). In contrast, the chlorinity in discharging fluids from Plume and Vent 3 sites did not change substantially from 1984 to 1994 (Table 1, Metz & Trefry, 2000; Trefry et al., 1994; Von Damm & Bischoff, 1987). Concentrations of Fe in Vent 1 hydrothermal fluids also decreased monotonically from 1984 to 2016 (Figure 3c). The endmember concentration of all but one measured solute from Vent 1 in 1984 decreased in samples collected in 2016 (Table 1). The one solute that did not decrease was sulfate, which remained depleted.

Radiocarbon ages of foraminifera tests in the three sediment cores are the median probabilities (in calibrated years before present, Table S9) from which the age of the bottom-most (basal) interval was estimated (Figures 1 and S1). This age provides an approximation of the minimum age for the underlying lava flow, which was not taken from the youngest flow that erupted from the Cleft because it contained too little sediment to core, but on older flows on the edge of the axial valley (e.g., Clague et al., 2013). The radiocarbon age of each 5-cm interval increases with depth in the three cores, as expected, suggesting that bioturbation is not a complicating factor. Cores T876-PC52 and T877-PC54 are 0.5 and 0.7 km from the axis of the spreading

Table 1
Endmember Compositions of Hydrothermal Discharge Sites From the Southern Cleft Segment of the Juan de Fuca Ridge

Vent	Seawater	Vent 1	Plume[a]	Vent 1[a]	Vent 3[a]	Seawater[a]	Plume[b]	Vent 1[b]	Vent 3[b]	Vent 1[b]	Vent 3[b]	Seawater[b]
Year	2016	2016	1984	1984	1984	1984	1990	1990	1991	1994	1994	1994
Temperature (Celsius)	2	338	224	285	11	11	246	332	332	342	214	2
Mg (mmol/kg)	52.3	1	0	0	0	52.7	-	-	-	-	-	-
Ca (mmol/kg)	10.1	67.9	96.4	84.7	77.3	10.2	-	-	-	-	-	-
Sr (μmol/kg)	89.2	241	312	230	267	87	-	-	-	-	-	-
Na (mmol/kg)	461	570	796	661	784	464	-	-	-	-	-	-
Chlorinity (mmol/kg)	542	756	1,090	896	951	541	1,140	806	946	792	946	546
K (mmol/kg)	9.9	33.5	51.6	37.3	45.6	9.8	-	-	-	-	-	-
Li (μmol/kg)	25.1	980	1720	1,110	1810	26	-	-	-	-	-	-
Sulfate (mmol/kg)	27.0	1.71	−0.5	−1.3	−1.7	27.9	-	-	-	-	-	-
Ba (μmol/kg)	0.15	73.1	-	-	-	-	-	-	-	-	-	-
Mn (mmol/kg)	0.0	1.47	3.59	2.61	4.48	<0.001	-	-	-	-	-	-
Fe (mmol/kg)	0.0	5.91	18.7	10.3	17.8	<0.001	20.1	8.5	12.8	8.5	12.8	-
Si (mmol/kg)	0.160	21.1	23.3	22.8	22.7	0.16	-	-	-	-	-	-
Rb (μmol/kg)	1.37	21.3	37	28	32	1.3	-	-	-	-	-	-
Cs (nmol/kg)	2.2	177	-	-	-	-	-	-	-	-	-	-
Y (nmol/kg)	0.33	4.9	-	-	-	-	-	-	-	-	-	-
Mo (nmol/kg)	100	19.6	-	-	-	-	−6	-	32	-	32	110
V (nmol/kg)	38.4	33.0	-	-	-	-	-	-	-	-	-	-
U (nmol/kg)	12.0	0.12	-	-	-	-	-	-	-	-	-	-
Be (nmol/kg)	-	-	95	150	150	0.02	-	-	-	-	-	-
Al (μmol/kg)	-	-	1.9	-	-	0.02	-	-	-	-	-	-
pH	-	-	3.2	-	-	7.8	-	-	-	-	-	-
Alkalinity (mmol/kg)	-	-	~0	~0	~0	2.3	-	-	-	-	-	-
B (μmol/kg)	405	480	491	-	-	419	-	-	-	-	-	-
H2S (mmol/kg)	-	-	3.5	~3	~4.4	0	1.3	-	2.7	-	2.7	0
Cu (μmol/kg)	-	-	<2	<2	<2	0.007	1.5	15	2	15.5	2	0.004
Zn (μmol/kg)	-	-	900	<600	-	0.01	780	360	469	374	469	0.006
Se (μmol/kg)	-	-	<1	<1	<1	2.5	-	-	-	-	-	-
As (nmol/kg)	-	-	-	-	-	-	650	260	-	-	-	23
Cd (nmol/kg)	-	-	-	-	-	-	910	408	375	385	375	0.7
Co (nmol/kg)	-	-	-	-	-	-	200	780	180	1,150	180	0.02
Pb (nmol/kg)	-	-	-	-	-	-	1,630	640	1000	730	1000	0.06
Ga (nmol/kg)	-	-	-	-	-	-	67	45	34	-	62	-
Tl (nmol/kg)	-	-	-	-	-	-	92	42	47	45	60	-

[a]Von Damm and Bischoff (1987). [b]Metz and Trefry (2000) and Trefry et al. (1994).

center with basal interval ^{14}C ages (and therefore the minimum ages of the underlying lava flows) of 14.1 Kyr at an average depth of 12.5 cm and 17.3 Kyr at an average depth 13 cm, respectively. The more distant core is 2.7 km from the spreading axis and its basal age is 22.5 Kyr at an average depth of 24.75 cm. Using the core lengths and extrapolated ages at the base of each core yields an average rate of sediment deposition of 1.12 cm/Kyr. The last flow erupted from the southern Cleft Segment is about 30%–40% sediment covered, which considering the flow morphology of sheet and lobate lava indicates perhaps a deposition of 0.5 cm of sediment. The observed thin sediment cover therefore suggests an approximate age of the most recent

basaltic flow ~400–500 years ago. This age is also consistent with rare observed nonvent sessile sponges, stalked crinoids, and bamboo corals on the flow, but in numbers and sizes less than observed on well-dated flows from Axial Seamount that are ~1,250 years old and have adequate sediment cover to core and date the underlying flows (Clague et al., 2019).

4. Discussion

The initial work conducted on southern Cleft Segment concluded that the high chloride concentration in the high-temperature fluid that discharged from the Plume site was, in part, a result of subsurface phase separation and segregation (Von Damm & Bischoff, 1987). They proposed that such a brine phase was entrained into an actively convecting hydrothermal system with a Mg- and sulfate-depleted fluid that had undergone high-temperature seawater-rock reactions. Similar conclusions were reached by Bischoff and Rosenbauer (1989) and Butterfield and Massoth (1994); however, the latter was based on observations of hydrothermal discharge sites on the northern Cleft Segment. The 400–500-year estimated age of the southern Cleft axial lava flow is consistent with the absence of a vapor phase fluid, even during the earliest fluid collection in 1984. We build upon these conclusions, models of hydrothermal circulation and reaction, and new chemical and thermal data from 2016 to illustrate thermal and chemical evolution of brine-dominated fluids, discern subcrustal hydrologic conditions that constrain the minimum temperature and depth of reaction, and estimate the composition of the stable Mg- and sulfate-depleted hydrothermal fluid at Vent 1. Then, we use a globally compiled database of seafloor hydrothermal fluid endmembers with chlorinities in excess of 700 mmol/kg and related fluids to document consistency in brine compositions from vastly different geologic settings of seafloor hydrothermal systems and differences among these fluids and higher temperature sourced fluids from related seawater-basalt interactions.

4.1. Rate of Change in Fluid Properties and Hydrothermal Processes

4.1.1. Temperature

Multiyear temperature records for hydrothermal discharge sites are not common. Repeated visits to several hydrothermal discharge sites have shown occasional variation, but not long-term systematic changes in the absence of magmatic disturbance. For example, Fornari et al. (1998) presented a 3-year continuous record with a temperature range of <10°C, consistent with the observed changes in a 7-year record of discrete measurements from Bio9, a hydrothermal discharge site at 9°N on the EPR. They also showed temperatures at BioVent changed by only 2°C (370°C–368°C), during a continuous 6-month deployment, and they observed temperature variations during a seismically active period, suggesting changes occurred as a result of a cracking front. However, Choi and Lowell (2015) suggest that continuous temperature measurements would not detect changes in basal heat input (e.g., cracking front) on a time scale of several years in their idealized simulations. In another continuous thermal record, Larson et al. (2009) showed temperature changes of several degrees during a 3-month deployment on the Endeavor Segment of the JFR. Unlike previous records, the sensor resolution was able to document tidal effects on discharge temperature and abrupt single degree Celsius deviations.

Except for the initial temperature measurement in 1984 when the pilot had difficulty placing the probe within orifices from which hydrothermal fluids discharged, the temperature record at Vent 1 has remained stable within a ~10°C range during a 26-year period (Figure 3a). In a portion of that record, continuous, hourly measured temperatures did not fluctuate more than a few degrees Celsius for a period of at least 3.3 years, and perhaps as long as 22 years. The near constant temperatures at Vent 1 and the lack of substantial earthquakes in the region during the past three decades (e.g., Dziak et al., 2011; Hildebrand et al., 1997) suggest a lack of physical changes to the hydrothermal circulation pattern within the southern Cleft Segment. Idealized simulations suggest a constancy in discharge temperature for decades with or without magma replenishments (Choi & Lowell, 2015); however, simulated temperatures using idealized parameters have a larger dynamic range than observed at Vent 1 and other discharge sites described above. This measure of consistency in the temperature of the discharging fluid points toward conductive heat transfer instead of active convection or a cracking front, which are dynamic processes in a heterogeneous system. Either would

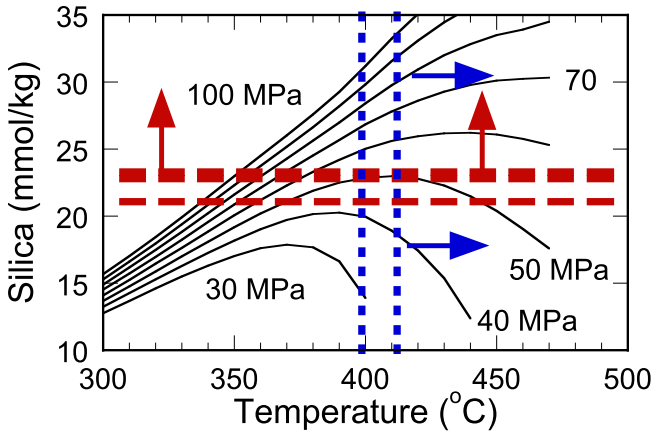

Figure 4. Dissolved silicon in hydrothermal fluids are plotted as a function of temperature, based on the formulation of Von Damm et al. (1991) using densities from Bischoff and Rosenbauer (1985). This representation is adequate for seawater-like salinities (e.g., Scheuermann et al., 2018). The red dashed lines represent measured concentrations in Plume (23.3 mmol/kg) and Vent 1 (22.8 mmol/kg) collected in 1984 (Von Damm & Bischoff, 1987) and Vent 1 (21.1 mmol/kg) collected in 2016. The blue dashed lines represent calculated temperatures using an Fe/Mn molar ratio (Plume—412°C in 1984; Vent 1—398°C–399°C in 1984 and 2016, both with a predicted error of ±10°C–13°C; Pester et al., 2011). The Fe/Mn data represent the most recent reaction conditions, thus the temperatures of brine formation are likely higher than calculated temperatures. The Si data from Plume in 1984 are consistent with a pressure of 44–49 MPa, at least 2.2 km below the seafloor. These are minimum values because we assume that Si is conservative during ascent as hydrothermal fluids cool before discharging at the seafloor.

likely affect discharge temperatures at various rates and magnitudes, especially over a three-decade-long period.

4.1.2. Solutes

Unlike temperature, the chlorinity in Vent 1 fluids decreased monotonically with time. Such results are consistent with sampling at most hydrothermal discharge sites in that temperatures of discharging fluids are often decoupled from estimates of temperature based on water-rock reactions and fluid compositions (e.g., Corliss et al., 1979; Larson et al., 2009; Wheat et al., 2017). Chlorinity at Vent 1 decreased from 65% higher than seawater in 1984 to 39% higher in 2016. The rate of change in chlorinity also decreased with time at Vent 1 from 15 mmol kg^{-1} $year^{-1}$ (1984–1990) to 3.5 mmol kg^{-1} $year^{-1}$ (1990–1994) to 1.6 mmol kg^{-1} $year^{-1}$ (1994–2016; Figure 3b). The observed decrease in chlorinity prior to a decrease in the temperature of discharging fluids is consistent with simulations by Choi and Lowell (2015) after single-phase conditions are established.

In contrast, there is a near-constant chlorinity of ~950 mmol/kg at Vent 3 (1984–1994) and ~1,100 mmol/kg at the Plume site (1984–1990), suggesting changes at Vent 1 are not uniform along this portion of the ridge segment. Here the three sampled discharge sites are within a distance of 5 km. Hydrothermal discharge from Plume and Vent 3 sites has not been sampled since 1994, so their longer-term chemical stability remains unknown; however, measured temperatures upon insertion of continuous temperature recorders and discrete probes remained relatively constant for ~15 years (Figure 3a).

Nonuniform results for the three hydrothermal sites were also observed in Fe concentrations in discharging fluids. Dissolved Fe in Vent 1 and Vent 3 fluids decreased with time accompanied by a decrease in the Fe/chlorinity molar ratio (Figure 3c). However, the Fe/Mn molar ratio remained strikingly uniform at Vent 1 (Table 1). Using a Fe/Mn geothermometer (Pester et al., 2011), the calculated reaction temperature at Vent 1 and Vent 3 is 398°C–399°C ± 10°C. In contrast, the 1984 sample from Plume had a calculated reaction temperature of 412°C ± 10°C that is near the two-phase boundary for seawater at a depth of ~3,100 m, which is ~900 m deeper than the seafloor (Bischoff & Rosenbauer, 1987). Such temperatures would require adiabatic cooling and conduction upon ascent to the seafloor to account for measured temperatures. These calculated reaction temperatures are considered minimum temperatures, because upon ascent when such fluids cool, if hydrothermal fluids reequilibrated or reacted with basalt, then likely reactions would lower the Fe/Mn molar ratio leading to a lower calculated temperature. Nevertheless, the chemical data point to a hot (>400°C) source for the brine-dominated fluid.

To assess the potential depth that such reactions may occur, we build on Von Damm and Bischoff (1987) who used a generic depth to the magma chamber of 2.3–2.5 km below the seafloor. This range is in agreement with those inferred using silica solubility data. The dissolved silicon concentration (23.3 mmol/kg) for Plume is well constrained by samples with Mg concentrations as low as 4 mmol/kg. In contrast, the lowest measured Mg value at Vent 1 in 1984 was ~22 mmol/kg with an endmember Si concentration of 22.8 ± 1.7 mmol/kg (interpolated from Figure 2g in Von Damm & Bischoff, 1987). This standard deviation encompasses the value measured in 2016 in which the lowest Mg concentration was 1 mmol/kg (Table 1). Because the reequilibrium of dissolved silica is slower than Fe or Mn upon cooling (Seewald & Seyfried, 1990), we use the Fe/Mn ratio to set the minimum temperature of reaction and use the silica data to estimate the minimum depth of reaction. Using the empirical equation of Von Damm et al. (1991), density determinations from Bischoff and Rosenbauer (1985), and data from Plume in 1984, the calculated pressure of reaction is at least 50 MPa (500 bars; Figure 4). In brine-dominated solutions such calculations introduce an error because of the density term, which has been updated by Driesner and Heinrich (2007). Using the formulation by Akinfiev and Diamond (2009), which provides a good match to silica solubility data in brine-dominated

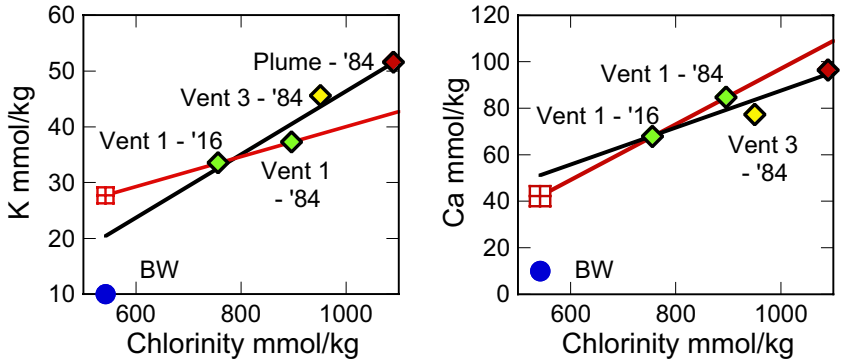

Figure 5. K and Ca plotted versus chlorinity in hydrothermal fluids from the southern Cleft Segment (Table 1). The black line is fitted to all four hydrothermal compositions whereas the red line is fitted to the two measurements from Vent 1. The red box with internal lines indicates an extrapolation to seawater chlorinities and is a measure of the Mg- and sulfate-depleted hydrothermal fluid that mixes with the deep-sourced brine. Bottom water (BW, blue filled circle) is shown for reference.

fluids (Scheuermann et al., 2018), the calculated pressure for Plume in 1984 is 44–49 MPa, assuming a standard error in the end member concentration of 1 mmol Si/kg. This pressure is equivalent to a depth that is at least 2.2 km below the seafloor at a water depth of ~2,240 m. Similar pressures are calculated for the Vent 1 data from 1984. Although the 1984 and 2016 Vent 1 Si endmember concentrations are statically identical, the lower dissolved silica value in 2016 is consistent with a shallower reaction equilibration zone. Nevertheless, such a zone would be at least 2 km below the seafloor, given the potential for silica precipitation during ascent (Akinfiev & Diamond, 2009). This depth is much deeper than known permeable zone in upper basaltic crust (e.g., Fisher, 1998) and likely near the base of the sheeted dike zone, or the top of the axial magma chamber (Morton et al., 1987).

4.2. Composition of the Stable Hydrothermal Fluid

After the intrusion of magma, hydrothermal systems display a range of characteristics that eventually lead to near constant or stable conditions for long periods of time (e.g., Butterfield et al., 1997). Many hydrothermal fluids have chlorinities and Na concentrations near bottom seawater concentrations. In addition, concentrations of Fe and Mn in stable fluids are typically orders of magnitude less than those observed in discharging fluid from Vent 1. Thus, the high concentrations of chlorinity, Na, Fe, and Mn in discharging fluids from Vent 1 are derived from a deep-sourced, brine-dominated fluid. Relative to the concentration in bottom seawater, chlorinity, Na, Fe, and Mn concentrations in discharging fluids from Vent 1 decreased on average by ~43% from 1984 to 2016. Assuming conservative behavior after mixing and during ascent, we use this proportional change and changes in concentrations of other solutes to calculate the composition of solutes in the stable hydrothermal fluid.

Unlike the four solutes mentioned above, changes in other solute concentrations decreased by ~25% for Ca and Rb and ~13% for Li and K from 1984 to 2016. These differences, compared to the 43% decrease in the other solutes, can be explained by a hydrothermal fluid that has previously reacted with basalt. Such water-rock reactions would result in the loss of seawater Mg and sulfate and a gain in dissolved K, Li, Rb, and Ca from basalt. Assuming that the observed change in Ca from 1984 to 2016 represents a 43% change in the contribution of the 1984 fluid, the calculated fluid composition of the stable fluid is 46 mmol Ca/kg (Figure 5). Similar calculations result in concentrations of 29 mmol K/kg, 810 μmol Li/kg, and 13 μmol Rb/kg for the stable fluid. Although the dissolved silicon is statistically analogous, a similar calculation results in a stable fluid with a 19 mmol Si/kg. This confirms a deep source for the stable fluid with a temperature-pressure combination that is cooler than the critical point, using the formulation developed by Von Damm and Bischoff (1987), which is suitable for near seawater chlorinities (Figure 4). Each of these concentrations is reasonable for a stable high-temperature hydrothermal fluid that has reacted with basalt.

Other solutes (Sr and B) are little changed from 1984 to 2016 in Vent 1 hydrothermal fluids. For example, Sr concentrations remained largely unchanged (230 ± 5 μmol/kg in 1984 compared with 241 ± 0.5 μmol/kg in 2016) and B concentrations are constant through time and nearly identical to seawater. This implies that the concentrations of these two solutes are nearly identical to concentrations in stable and brine-dominated fluids.

We speculate that in centuries prior to 1984, a magmatic event occurred resulting in an eruption on the seafloor (Eaby et al., 1984) that may have been accompanied with replenishment of the magma chamber and/or dike injection(s). This magmatic event resulted in phase separation and brine accumulation in the crust. While the vapor phase discharged, the dense brine phase remained, likely stored in pore spaces, cracks, and fissures that are not well connected near the base of the sheeted dikes, or deeper. Since 1984, and likely for decades or centuries prior, this brine has mixed with or diffused into a stable Mg- and sulfate-depleted hydrothermal system (e.g., Bischoff & Rosenbauer, 1987; Coumou et al., 2009). Given the lack of seismic activity along this ridge segment (e.g., Hildebrand et al., 1997), the stable hydrothermal system is thought to be slowly using up the deep-sourced brine reservoir and no further magma replenishments have occurred since this portion of the ridge last erupted. Therefore, the presently active hydrothermal system is likely a stable seawater-recharged convective system driven by residual heat from the last magmatic perturbation with a decreasing contribution from the residual brine that was stored in the deep subsurface shortly after the magmatic event.

4.3. Assessing a Brine Composition

Discharging hydrothermal fluids from the northern Cleft Segment represent the highest chlorinity (1,245 mmol/kg) measured on a MOR (Butterfield & Massoth, 1994). This is equivalent to an 8 weight percent (wt%) NaCl solution. At its maximum, discharging fluids from Vent 1 were at most a 5.8 wt% NaCl equivalent solution. Such salt contents are consistent with modeled discharging fluids with the average maximum salt content of ~6 wt% and a maximum of 9 wt% (Schoofs & Hansen, 2000). Discharge of brines with higher (10–25 wt% NaCl) salinities is possible, based on the force exerted by the integrated density of a recharging cold hydrostatic fluid pathway (Fontaine & Wilcock, 2006; Fontaine et al., 2007). Much higher salt solutions are predicted during high-temperature phase separation, with possible solutions in the range of 30–60 wt% (Choi & Lowell, 2015). Fluid inclusion data from oceanic and ophiolitic dike and gabbro samples support the existence of such high, and many lower, salt solutions in inclusions that formed at temperatures from 150°C to 525°C (e.g., Castelain et al., 2014; Cowan & Cann, 1988; Kelley & Robinson, 1990; Kelley et al., 1993; Nehlig, 1991). Fluid inclusions were recently recovered in Icelandic basaltic dikes from the hydrothermal reaction zone of an active, seawater-recharged hydrothermal system (Bali et al., 2020). Co-existing vapor-phase and brine-filled inclusions homogenize at 600°C ± 20°C (e.g., Bali et al., 2020). These brine inclusions have a chlorinity of 7,100 mmol/kg (Table 2), more than an order of magnitude greater than the recharging seawater concentration.

Additional evidence for high-salinity brines in basalt-hosted seawater-recharged hydrothermal systems stems from the assimilation of such brine in the underlying magma that later erupts and solidifies with the additional brine component (e.g., Coombs et al., 2004; Kent et al., 1999; Michael & Cornell, 1998). Brines that were incorporated into Kilauea basaltic glasses, for example, had a chlorinity of ~3,600 mmol/kg (~23 wt% NaCl; Coombs et al., 2004; Table 2).

We use both data types (fluid inclusions and brine assimilation) to characterize the composition of the deep-sourced brine in the southern Cleft Segment. If we consider a chlorinity of 7,100 mmol/kg (fluid inclusion) as the concentration in the deep-seated brine and the estimated chlorinity of 540 mmol/kg as the stable basalt-hosted hydrothermal composition, then the percentage of brine in fluids collected from Plume in 1984 was only 8.4% brine. Similarly, in 1984 the Vent 1 fluid was only 5.4% brine, decreasing to 4.0% in 1990 and 3.8% in 1991. The proportion of brine is more than twice as high if the deep-sourced brine instead had a chlorinity of 3,600 mmol/kg, which reflects the composition of fluids that were assimilated into Kilauea basalts (Coombs et al., 2004). Thus, extrapolating to the composition of the deep-sourced brine using the composition of discharged fluids from only Vent 1 or from each of the three discharge sites on the southern Cleft Segment is a significant extrapolation. Therefore, the following projected outcomes should be considered primarily in a qualitative context.

Table 2
Measured and Calculated Concentrations of Hydrothermal Brines

Element unit	Fluid inclusion	Assimilation in basalt	Vent 1	Southcleft	Bottom seawater
NaCl[a] (wt %)	54	23	42	42	3.5
Na (mmol/kg)	2,200	1,900	4,700	5,100	461
Cl (mmol/kg)	7,100	3,600	7,100	7,100	542
K (mmol/kg)	1,800	660	200	390	9.9
Li (mmol/kg)	-	-	6.9	17	0.026
Rb (μmol/kg)	4.9	940	330	320	1.37
Cs (nmol/kg)	-	-	-	~2,000	2.20
Ca (mmol/kg)	450	650	830	570	10.1
Mn (mmol/kg)	150	-	53	47	<0.01
Fe (mmol/kg)	1,800	-	200	240	<0.01
Mg (mmol/kg)	0.01	-	0	0	52.3
Sr (μmol/kg)	-	-	-	1,800	87.0
Ba (μmol/kg)	9.20	4,500	-	-	0.2
Pb (μmol/kg)	NA	34	-	-	-
B (μmol/kg)	1.50	NA	-	-	400
Na/Cl (mmol/mmol)	0.31	0.53	0.66	0.72	0.85
Na/K (mmol/mmol)	1.2	2.9	24	13	47
Na/Rb (mmol/μmol)	445	2	14	16	340
Na/Ca (mmol/mmol)	4.9	2.9	5.7	8.9	46
Fe/Mn((mmol/mmol)	12	-	3.8	5.1	-
Ca/Cl (mmol/mmol)	0.063	0.181	0.117	0.080	0.019
Charge balance[a] (mmol/kg)	−1,700	−261	27	−121	−57

Note. Measured data stem from analyses of fluid inclusion from a deep borehole in Iceland that intersected the hydrothermal reaction zone at ~600°C and from assimilation of brines in basalts from Kilauea (Bali et al., 2020; Coombs et al., 2004). Calculated concentrations are based on data from only Vent 1 and from all three sampled on the southern Cleft Segment. Calculated results were adjusted to a chlorinity of 7,100 mmol/kg.

[a]Weight percent equivalent of NaCl.

To provide a measure of the potential range in the composition of the deep-seated brines, we used the composition of fluids from Vent 1 (green line in Figure 6, Table 1) and from all three of the discharge sites on the southern Cleft Segment (blue line in Figure 6, Table 1) to calculate the composition of the deep-source brine, assuming conservative (linear) behavior and given a chlorinity of 7,100 mmol/kg for the deep-sourced brine (Table 2). We performed both calculations because the three discharge sites on the southern Cleft Segment are separated by nearly 5 km and there is no direct evidence that all three have a linked hydrologic source. However, modeled systems predict discharge sites should be spaced at half the depth of the circulation cell (Cherkaoui & Wilcock, 2001). Given the minimum depth from the silica data of >2.2 km, which is consistent with the dike/magma lens transition at ~2.5-km depth (Morton et al., 1987), a spacing of 1.4 km may allow for some interconnectivity of the three discharge sites. Nevertheless, results from both calculated brine compositions are generally similar for most solutes; however, the calculation that used data from each of the three discharge sites on the southern Cleft Segment benefited from more data, including samples from Plume that have a greater percentage of the brine component (Figure 6, Table 1). The similarity in these results suggests that either the hydrologic pathways are linked or the reaction and transport processes below the three discharge sites are similar.

Another measure for the potential range in the deep-sourced brine composition is the relationship between the data from the southern Cleft Segment and endmember data collected from 23 hydrothermal discharge sites from around the globe with chlorinities in excess of 700 mmol/kg (Mottl, 2012) and 10 endmember

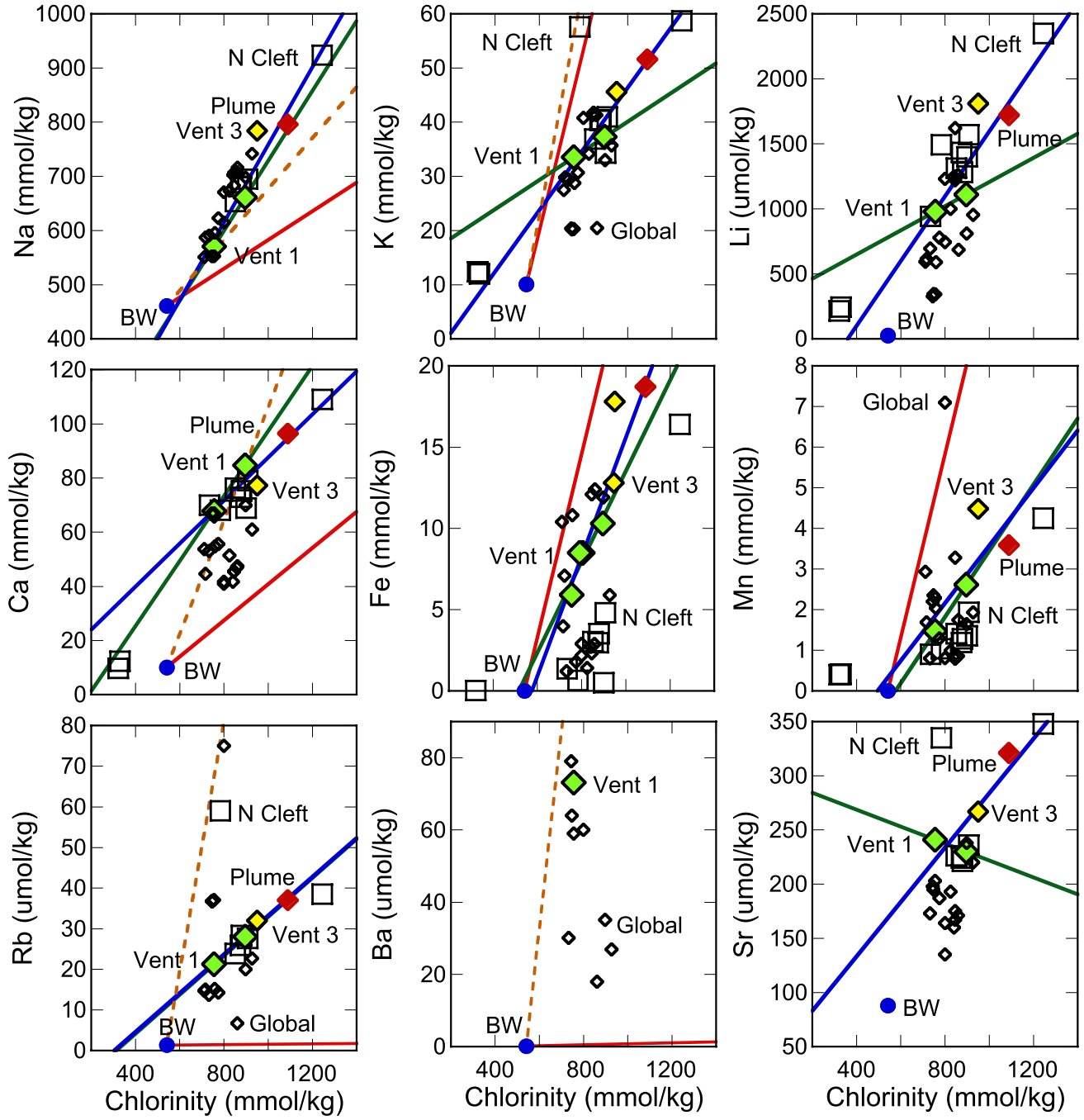

Figure 6. Concentrations of bottom seawater (blue filled circle, BW) and endmember hydrothermal fluids from the southern Cleft Segment (colored symbols from Vent 1 [light green], Vent 3 [yellow], and Plume [red]), northern Cleft Segment (open squares, Butterfield & Massoth, 1994), and other hydrothermal fluids with chlorinities greater than 700 mmol/kg and listed in Vent DB (open diamonds, Mottl, 2012). Data from the south Cleft Segment are from Von Damm and Bischoff (1987), Trefry et al. (1994), Metz and Trefry (2000), and this work (Table 1). The blue line is the best fit to the data from the southern Cleft Segment and the green line to the Vent 1 data. The red line connects the composition of a brine within fluid inclusions (Bali et al., 2020) to seawater concentrations (Table 2). The dashed orange line connects the composition of an assimilated brine (Kilauea lavas; Coombs et al., 2004) to seawater (Table 2)

fluid compositions from the northern Cleft Segment, where all but two datum have chlorinities in excess of 700 mmol/kg (Butterfield & Massoth, 1994; Figure 6). For example, in the plot of Na versus chlorinity, all of the data from endmember fluid compositions lie on the two lines defined by Vent 1 and data from the southern Cleft Segment, even though the geologic settings differed greatly from the ultramafic-hosted Rainbow

site on the slow spreading Mid-Atlantic Ridge, to fast and superfast spreading sites at 13°N, 9°N, and 18°S on the basalt-hosted EPR, to back-arc discharge at Vai Lili in Lau Basin with a basalt-andesite foundation. This linear Na-chlorinity relationship likely represents a uniform reaction process or equilibrium at depth associated with the formation of a hypersaline brine by phase separation and segregation.

This global compilation of hydrothermal data can also be compared with fluid inclusion and brine assimilation data. The Iceland geothermal system is a long-lived (>10 ka) system. Paragenetically constrained, mineral geothermometry tracks hydrothermal alteration from near magmatic temperatures to the present-day system with *in situ* temperatures of 600°C (Bali et al., 2020; Zierenberg et al., 2019). The bulk of the alteration in these rocks occurred at ~800°C, and the rocks were pervasively altered. Likewise, brines assimilated into basalt also must experience similar high temperatures, but the fluid likely formed as a seawater-sourced brine prior to incorporation into the magma. In contrast, discharge from hydrothermal systems on most seafloor spreading systems is generally considered to be significantly cooler, thus a systematic change in fluid composition from hydrothermal fluid to basalt assimilation to Icelandic fluid inclusions could be anticipated based on reactions at successively higher temperatures. The composition of these two fluids (inclusion and assimilated, Table 2) is illustrated in Figure 6 as solid red (fluid inclusion) or dashed orange (brine assimilation) lines drawn through the composition of bottom seawater.

Because Na and Cl are the two primary elements in the brine, the Na versus chlorinity relationship is dominated by dilution. However, relative to the hydrothermal discharge data, the assimilated brine and fluid inclusions have a significantly lower Na/Cl molar ratio (Figure 6, Table 2). A lower ratio is expected at high temperatures in which Na in the hydrothermal fluid is exchanged for Ca in the rock due to plagioclase reaction and conversion of clinopyroxene to hornblende (Bali et al., 2020; Fridleifsson et al., 2020; Zierenberg et al., 2019). A consistency of brine-forming temperatures is warranted because higher temperature reactions would result in additional exchange of Na, which would lower the Na/chlorinity molar ratio of the hydrothermal fluid and result in a range of Na/chlorinity molar ratios. This is inconsistent with the observed linear Na-chlorinity trend from the global hydrothermal data set (Figure 6), but is consistent with observed fluid assimilation and inclusion data that reacted at higher temperatures. This result points to a temperature-dependent equilibrium condition in which the temperature of brine formation is globally consistent.

Given (1) the chlorinity is not expected to change in the brine as a result of continued reaction after brine formation, but Na and other solutes could continue to exchange with host rock, (2) relationships between solutes (with the exception of Fe) and chlorinity are linear, and (3) the 32-year record of brine discharge at Vent 1, together these results suggest that there is minimal brine-rock exchange even for periods of decades to centuries in which the brine may reside in the crust at temperatures in excess of 400°C. Thus, residence time does not appear to play a significant role in controlling the major ion composition of brines in typical MOR environments, consistent with numerous high-temperature laboratory experiments that reach equilibrium within months of initiating the experiment (e.g., Seyfried & Mottl, 1982).

The plot of Ca versus chlorinity shows a similar grouping of the four projections with more scatter in the hydrothermal data relative to Na (Figure 6). Pester et al. (2015) demonstrated that the Ca/Cl molar ratio increases with increasing Cl due to the solubility of plagioclase, and data from Vent 1 fall in the range indicative of a host rock with plagioclase of An_{75} (% anorthite). This value is consistent with plagioclase content in the most recently erupted basalt that covers the seafloor on the southern Cleft Segment (Eaby et al., 1984). Given the observed increase in Ca/Cl with increasing Cl, our projected linear response underestimates the Ca concentration in the deep-sourced brine, which is probably closer to the value derived from the brine assimilated into basalt (Table 2). The Na/Ca molar ratio decreases by a factor of 5–16 from the bottom seawater value reflecting exchange reactions, noted above.

Hydrothermal K data deviate little from a line based on the data from the southern Cleft Segment with the fluid inclusion and brine assimilation data supporting higher K/Cl molar ratios (Figure 6). Fluid inclusion and brine assimilation data also support a much lower Na/K molar ratio than that of seawater with the hydrothermal data spanning the two extremes (Table 2). Fluid inclusions from Iceland have lower Na and higher K than extrapolated values from south Cleft data suggesting more extensive alteration of plagioclase and replacement of clinopyroxene by hornblende, both of which involve the uptake of Na in the alteration minerals and the release of K to the fluid (Bali et al., 2020).

Two other alkali metals (Li and Rb) show consistent trending slopes based on the hydrothermal data, but only Rb was measured in the fluid inclusions and brine-assimilated basalt (Table 2, Figure 6). The inclusion and assimilated Rb data do not represent the hydrothermal data with the exception of several high Rb concentrations from Vai Lili, Rainbow, and a diffuse discharge site from the northern Cleft Segment. These three samples trend with the brine assimilated data, but not the inclusion data. In contrast, the Ba and Sr data highlight the difficulty in predicting the brine composition based on few data (e.g., Ba) and differences in concentrations that are near the limits of precision for analytical procedures (e.g., Vent 1, Sr; Figure 6).

Fe concentrations in the calculated deep-sourced brine from the southern Cleft Segment are lower than values measured in fluid inclusions (by about an order of magnitude), consistent with reduced mineral alteration in the brine from the southern Cleft Segment (Table 2). Another measure of more extensive reaction is provided by the Fe/Mn molar ratio. In Icelandic fluid inclusions the Fe/Mn is 12 (mol/mol), about twice the ratio calculated for data from the southern Cleft Segment (5.1, Table 2). The Fe/Mn molar ratio of basalt is ~53, again indicating more complete reaction in Icelandic brines relative to hydrothermal fluids. Zierenberg et al. (2019), show that magnetite and ilmenite record equilibrium values of Mn and Fe at ~620°C, which is approximately 20°C–30°C higher than the estimated in situ temperature when the rocks were recovered by drilling. As a group, the hydrothermal Fe endmember values do not support a single trend like the other elements, possibly indicating two distinct trends. Two trends could suggest a difference in reaction temperature with the Fe-rich and higher Fe/chlorinity sites having a hotter source, based on the model by Pester et al. (2011) and the single trend in the Mn versus chlorinity data.

Together, these data suggest that the composition of a subseafloor hydrothermal brine will likely change as a function of temperature within the basaltic crust, assuming an increase in the temperature of reaction from the global hydrothermal data set to brine assimilation to fluid inclusions within the Icelandic reaction zone. The hydrothermal data also group together with variations in source rock composition, suggesting equilibrium is controlled by a similar suite of alteration minerals at depth even in different hydrologic and geologic settings.

5. Conclusions

Three hydrothermal discharge sites were discovered in 1984 on the southern Cleft Segment of the JFR and were still active in 2016: Vent 1, Plume, and a site 300 m NNE along the fissure from Plume. We present new chemical and thermal data from discharging hydrothermal fluids from Vent 1. These data extend the record for a brine-dominated discharging fluid to 32 years. The most remarkable aspect of these data is that the chlorinity of discharging fluids has retained a brine influence after brine segregated due to a magmatic event that likely occurred centuries prior to discovery of the hydrothermal systems in 1984. Vapor-dominated fluids would have initially discharged shortly after the magmatic event, as witnessed a few years later after an eruption on the northern Cleft Segment (Butterfield & Massoth, 1994). This vapor-dominated phase would be followed by the discharge of high-chlorinity, brine-dominated fluids, as measured in 1984 (Von Damm & Bischoff, 1987). Since 1984, the chlorinity of hydrothermal fluids that discharge from Vent 1 has decreased while the temperature has remained relatively uniform during the past 22 years or longer. We contend that the discharging fluid composition is a mixture of a stable, Mg- and sulfate-depleted altered seawater and a brine component (probably <10%). Data from the southern Cleft Segment and a global compilation of more than 30 endmember fluids with chlorinities in excess of 700 mmol/kg were used to constrain the composition of stable and brine-dominated hydrothermal fluids.

Hydrothermal brines are similar in many ways to compositions of fluid inclusions and brines assimilated in magmas, but there are differences in the extent of fluid alteration, with the most altered fluids being those from fluid inclusions in a reaction zone within Icelandic basalt (Bali et al., 2020). The extent of reaction is likely influenced by temperature, and residence time does not appear to be an important factor in shaping the brine composition. Prior to collection in 2016, brines below Vent 1 likely resided within the crust for at least four decades and maybe for centuries, consistent with geologic evidence of a seafloor eruption prior to the first observations in 1984 (Eaby et al., 1984). Worldwide element-chlorinity data for discharging hydrothermal fluids with chlorinates in excess of 700 mmol/kg show uniform linear trends even though crustal, hydrologic, and magmatic conditions differ. This result points to a process or condition (e.g., temperature) that is uniform through these varied geologic settings.

Lastly, the longevity of hydrothermal systems varies depending on magma supply with models indicating that hydrothermal discharge at MORs can last for centuries. Studies over much of the past two decades have focused on hydrothermal systems that are vapor dominated, stemming from the excitement of recent magmatic inputs. However, vapor-dominated discharge is relatively short lived in comparison to the potential for century-long discharge of brine-dominated and stable Mg- and sulfate-depleted fluids. Given the different potentials for metal mobilization of vapor-, brine-, and stable-dominant fluids, fluxes and chemical budgets should consider the volumetric partitioning among these fluids over the lifetime of MOR activity.

Data Availability Statement

The DSL-120 data are available through the Marine Geoscience Data System, with DOI 10.26022/IEDA/329822 for the DSL-120 processed files; DOI 10.26022/IEDA/329817 for netCDF grids, DOI 10.26022/IEDA/329818 for ASCII raster files, and DOI 10.26022/IEDA/329819 for geoTiffs of bathymetry data; and DOI 10.26022/IEDA/329820 for netCDF grids and DOI 10.26022/IEDA/329821 for geoTiffs of backscatter data. More detailed maps and all new temperature and fluid data are provided in Supporting Information and archived at DOI https://doi.org/10.5281/zenodo.4047101.

Acknowledgments
The authors thank the shipboard parties for their contributions at sea, including the crews and pilots of the MBARI ROVs *Tiburon* and *Doc Ricketts* and R/V *Western Flyer*. They also thank the WHOI Deep Submergence Group for collecting the DSL-120 data. The format and quality of this manuscript was greatly improved by comments from Jeff Seewald, Joris Gieskes, and an anonymous reviewer. This research was supported by National Science Foundation grants OCE-1536623 (CGW) and grant OIA-0939564 to the Center for Dark Energy Biosphere Investigations (C-DEBI) Science and Technology Center, and the David and Lucile Packard Foundation, which supported the DSL data collection and processing and fluid and sulfide collection in 2016. This is C-DEBI contribution 546. There are no real or perceived financial conflicts of interests for any author.

References

Akinfiev, N. N., & Diamond, L. W. (2009). A simple predictive model of quartz solubility in water–salt–CO_2 systems at temperatures up to 1000 C and pressures up to 1000 MPa. *Geochimica et Cosmochimica Acta*, *73*(6), 1597–1608. https://doi.org/10.1016/j.gca.2008.12.011

Baker, E. T., Massoth, G. J., & Feely, R. A. (1987). Cataclysmic hydrothermal venting on the Juan de Fuca Ridge. *Nature*, *329*(6135), 149–151.

Baker, E. T., Massoth, G. J., Feely, R. A., Embley, R. W., Thomson, R. E., & Burd, B. J. (1995). Hydrothermal event plumes from the CoAxial seafloor eruption site, Juan de Fuca Ridge. *Geophysical Research Letters*, *22*(2), 147–150.

Bali, E., Aradi, L. E., Zierenberg, R., Diamond, L. W., Pettke, T., Szabó, A., et al. (2020). Geothermal energy and ore formation potential of 600°C mid-ocean ridge hydrothermal fluids. *Geology*. https://doi.org/10.1130/G47791.1

Bischoff, J. L., & Rosenbauer, R. J. (1985). An empirical equation of state for hydrothermal seawater (3.2 percent NaCl). *American Journal of Science*, *285*(8), 725–763.

Bischoff, J. L., & Rosenbauer, R. J. (1987). Phase separation in seafloor geothermal systems; an experimental study of the effects on metal transport. *American Journal of Science*, *287*(10), 953–978.

Bischoff, J. L., & Rosenbauer, R. J. (1989). Salinity variations in submarine hydrothermal systems by layered double-diffusive convection. *The Journal of Geology*, *97*(5), 613–623.

Butterfield, D. A., Jonasson, I. R., Massoth, G. J., Feely, R. A., Roe, K. K., Embley, R. E., et al. (1997). Seafloor eruptions and evolution of hydrothermal fluid chemistry. *Philosophical Transactions of the Royal Society of London. Series A: Mathematical, Physical and Engineering Sciences*, *355*(1723), 369–386.

Butterfield, D. A., & Massoth, G. J. (1994). Geochemistry of north Cleft segment vent fluids: Temporal changes in chlorinity and their possible relation to recent volcanism. *Journal of Geophysical Research: Solid Earth*, *99*(B3), 4951–4968.

Butterfield, D. A., McDuff, R. E., Mottl, M. J., Lilley, M. D., Lupton, J. E., & Massoth, G. J. (1994). Gradients in the composition of hydrothermal fluids from the Endeavour segment vent field: Phase separation and brine loss. *Journal of Geophysical Research: Solid Earth*, *99*(B5), 9561–9583.

Castelain, T., McCaig, A. M., & Cliff, R. A. (2014). Fluid evolution in an oceanic core complex: A fluid inclusion study from IODP hole U1309 D—Atlantis Massif, 30° N, mid-Atlantic Ridge. *Geochemistry, Geophysics, Geosystems*, *15*(4), 1193–1214. https://doi.org/10.1002/2013GC004975

Chadwick, W. W., Embley, R. W., & Fox, C. G. (1991). Evidence for volcanic eruption on the southern Juan de Fuca Ridge between 1981 and 1987. *Nature*, *350*(6317), 416–418.

Chadwick, W. W., Jr. (2016). High-temperature time-series raw data from hydrothermal vents at South Cleft, Juan de Fuca Ridge, acquired from 1999 to the present (investigator William Chadwick). *Interdisciplinary Earth Data Alliance (IEDA)*. https://doi.org/10.1594/IEDA/322430

Chadwick, W. W., Jr., Scheirer, D. S., Embley, R. W., & Johnson, H. P. (2001). High-resolution bathymetric surveys using scanning sonars: Lava flow morphology, hydrothermal vents, and geologic structure at recent eruption sites on the Juan de Fuca Ridge. *Journal of Geophysical Research: Solid Earth*, *106*(B8), 16075–16099.

Cherkaoui, A. S., & Wilcock, W. S. (2001). Laboratory studies of high Rayleigh number circulation in an open-top Hele-Shaw cell: An analog to mid-ocean ridge hydrothermal systems. *Journal of Geophysical Research: Solid Earth*, *106*(B6), 10983–11000.

Choi, J., & Lowell, R. P. (2015). The response of two-phase hydrothermal systems to changing magmatic heat input at mid-ocean ridges. *Deep Sea Research Part II: Topical Studies in Oceanography*, *121*, 17–30. https://doi.org/10.1002/ggge.20109

Clague, D. A., Dreyer, B. M., Paduan, J. B., Martin, J. F., Chadwick, W. W., Caress, D. W., et al. (2013). Geologic history of the summit of axial Seamount, Juan de Fuca Ridge. *Geochemistry, Geophysics, Geosystems*, *14*(10), 4403–4443. https://doi.org/10.1002/ggge.20240

Clague, D. A., Martin, J. F., Paduan, J. B., Butterfield, D. A., Jamieson, J. W., Le Saout, M., et al. (2020). Hydrothermal chimney distribution on the Endeavour segment, Juan de Fuca Ridge. *Geochemistry, Geophysics, Geosystems*, *21*, e2020GC008917. https://doi.org/10.1029/2020GC008917

Clague, D. A., Portner, R. A., Paduan, J. B., Le Saout, M., & Dreyer, B. M. (2019). Formation of the summit Caldera at Axial Seamount. Abstract V43C-0217, presented at 2019 Fall Meeting, AGU. San Francisco, CA.

Coombs, M. L., Sisson, T. W., & Kimura, J. I. (2004). Ultra-high chlorine in submarine Kılauea glasses: Evidence for direct assimilation of brine by magma. *Earth and Planetary Science Letters*, *217*(3–4), 297–313. http://dx.doi.org/10.1016/j.dsr2.2015.05.005

Corliss, J. B., Dymond, J., Gordon, L. I., Edmond, J. M., von Herzen, R. P., Ballard, R. D., et al. (1979). Submarine thermal springs on the Galapagos Rift. *Science*, *203*(4385), 1073–1083.

Coumou, D., Driesner, T., Weis, P., & Heinrich, C. A. (2009). Phase separation, brine formation, and salinity variation at Black Smoker hydrothermal systems. *Journal of Geophysical Research: Solid Earth*, *114*(B3). https://doi.org/10.1029/2008JB005764

Cowan, J., & Cann, J. (1988). Supercritical two-phase separation of hydrothermal fluids in the Troodos ophiolite. *Nature*, *333*(6170), 259–261.

D'Asaro, E., Walker, S., & Baker, E. (1994). Structure of two hydrothermal megaplumes. *Journal of Geophysical Research: Solid Earth*, *99*(C10), 20361–20373.

Delaney, J. R., Mogk, D. W., & Mottl, M. (1987). Quartz-cemented breccias from the Mid-Atlantic Ridge: Samples of a high-salinity hydrothermal upflow zone. *Journal of Geophysical Research: Solid Earth*, *92*(B9), 9175–9192.

DeMets, C., Gordon, R. G., & Argus, D. F. (2010). Geologically current plate motions. *Geophysical Journal International*, *181*(1), 1–80. https://doi.org/10.1111/j.1365-246X.2009.04491.x

Driesner, T. (2007). The system H2O–NaCl. Part II: Correlations for molar volume, enthalpy, and isobaric heat capacity from 0 to 1000 C, 1 to 5000 bar, and 0 to 1 XNaCl. *Geochimica et Cosmochimica Acta*, *71*(20), 4902–4919.

Dziak, R. P., Chadwick, W. W., Jr., Fox, C. G., & Embley, R. W. (2003). Hydrothermal temperature changes at the southern Juan de Fuca Ridge associated with MW 6.2 Blanco Transform earthquake. *Geology*, *31*(2), 119–122. https://doi.org/10.1130/0091-7613(2003)031<0119:HTCATS>2.0.CO;2

Dziak, R. P., Hammond, S. R., & Fox, C. G. (2011). A 20-year hydroacoustic time series of seismic and volcanic events in the Northeast Pacific Ocean. *Oceanography*, *23*(3), 280–293. https://doi.org/10.5670/oceanog.2011.79

Eaby, J., Clague, D. A., & Delaney, J. R. (1984). Sr isotopic variations along the Juan de Fuca Ridge. *Journal of Geophysical Research: Solid Earth*, *89*(B9), 7883–7890.

Embley, R. W., & Chadwick, W. W., Jr. (1994). Volcanic and hydrothermal processes associated with a recent phase of seafloor spreading at the northern Cleft segment: Juan de Fuca Ridge. *Journal of Geophysical Research: Solid Earth*, *99*(B3), 4741–4760.

Embley, R. W., Chadwick, W., Perfit, M. R., & Baker, E. T. (1991). Geology of the northern Cleft segment, Juan de Fuca Ridge: Recent lava flows, sea-floor spreading, and the formation of megaplumes. *Geology*, *19*(8), 771–775.

Fisher, A. T. (1998). Permeability within basaltic oceanic crust. *Reviews of Geophysics*, *36*(2), 143–182.

Fontaine, F. J., & Wilcock, W. S. (2006). Dynamics and storage of brine in mid-ocean ridge hydrothermal systems. *Journal of Geophysical Research: Solid Earth*, *111*(B6). https://doi.org/10.1029/2005JB003866

Fontaine, F. J., Wilcock, W. S., & Butterfield, D. A. (2007). Physical controls on the salinity of mid-ocean ridge hydrothermal vent fluids. *Earth and Planetary Science Letters*, *257*(1–2), 132–145. https://doi.org/10.1016/j.epsl.2007.02.027

Fornari, D. J., Shank, T., Von Damm, K. L., Gregg, T. K. P., Lilley, M., Levai, G., et al. (1998). Time-series temperature measurements at high-temperature hydrothermal vents, East Pacific Rise 9 49′–51′ N: Evidence for monitoring a crustal cracking event. *Earth and Planetary Science Letters*, *160*(3–4), 419–431.

Fornari, D. J., Von Damm, K. L., Bryce, J. G., Cowen, J. P., Ferrini, V., Fundis, A., et al. (2012). The East Pacific Rise between 9 N and 10 N: Twenty-five years of integrated, multidisciplinary oceanic spreading center studies. *Oceanography*, *25*(1), 18–43. https://doi.org/10.5670/oceanog.2012.02

Foustoukos, D. I., & Seyfried, W. E., Jr. (2007). Quartz solubility in the two-phase and critical region of the NaCl–KCl–H2O system: Implications for submarine hydrothermal vent systems at 9 50′ N East Pacific Rise. *Geochimica et Cosmochimica Acta*, *71*(1), 186–201. https://doi.org/10.1016/j.gca.2006.08.038

Fox, C. G., Chadwick, W. W., Jr., & Embley, R. W. (1992). Detection of changes in ridge-crest morphology using repeated multibeam sonar surveys. *Journal of Geophysical Research: Solid Earth*, *97*(B7), 11149–11162.

Friðleifsson, G. Ó., Elders, W. A., Zierenberg, R. A., Fowler, A. P. G., Weisenberger, T. B., Mesfin, K. G., et al. (2020). The Iceland Deep Drilling Project at Reykjanes: Drilling into the root zone of an analog of a black smoker. *Journal of Volcanology and Geothermal Research*, *391*, 106435. https://doi.org/10.1016/j.jvolgeores.2018.08.013

Han, L., Lowell, R. P., & Lewis, K. C. (2013). The dynamics of two-phase hydrothermal systems at a seafloor pressure of 25 MPa. *Journal of Geophysical Research: Solid Earth*, *118*(6), 2635–2647. https://doi.org/10.1002/jgrb.50158

Hildebrand, J. A., McDonald, M. A., & Webb, S. C. (1997). Microearthquakes at intermediate spreading-rate ridges: The cleft segment megaplume site on the Juan de Fuca Ridge. *Bulletin of the Seismological Society of America*, *87*(3), 684–691.

Humphris, S. E., & Klein, F. (2018). Progress in deciphering the controls on the geochemistry of fluids in seafloor hydrothermal systems. *Annual Review of Marine Science*, *10*, 315–343. https://doi.org/10.1146/annurev-marine-121916-063233

Kelley, D. S., Gillis, K. M., & Thompson, G. (1993). Fluid evolution in submarine magma-hydrothermal systems at the Mid-Atlantic Ridge. *Journal of Geophysical Research: Solid Earth*, *98*(B11), 19579–19596.

Kelley, D. S., & Robinson, P. T. (1990). Development of a brine-dominated hydrothermal system at temperatures of 400–500 C in the upper level plutonic sequence, Troodos ophiolite, Cyprus. *Geochimica et Cosmochimica Acta*, *54*(3), 653–661.

Kent, A. J., Clague, D. A., Honda, M., Stolper, E. M., Hutcheon, I. D., & Norman, M. D. (1999). Widespread assimilation of a seawater-derived component at Loihi Seamount, Hawaii. *Geochimica et Cosmochimica Acta*, *63*(18), 2749–2761.

Larson, B. I., Lilley, M. D., & Olson, E. J. (2009). Parameters of subsurface brines and hydrothermal processes 12–15 months after the 1999 magmatic event at the Main Endeavor Field as inferred from in situ time series measurements of chloride and temperature. *Journal of Geophysical Research: Solid Earth*, *114*(B1). https://doi.org/10.1029/2008JB005627

Lilley, M. D., Butterfield, D. A., Lupton, J. E., & Olson, E. J. (2003). Magmatic events can produce rapid changes in hydrothermal vent chemistry. *Nature*, *422*(6934), 878–881. https://doi.org/10.1038/nature01569

Lowell, R. P., & Germanovich, L. N. (1995). Dike injection and the formation of megaplumes at ocean ridges. *Science*, *267*(5205), 1804–1807.

Magenheim, A. J., Spivack, A. J., Michael, P. J., & Gieskes, J. M. (1995). Chlorine stable isotope composition of the oceanic crust: Implications for Earth's distribution of chlorine. *Earth and Planetary Science Letters*, *131*(3–4), 427–432.

Massoth, G. J., Butterfield, D. A., Lupton, J. E., McDuff, R. E., Lilley, M. D., & Jonasson, I. R. (1989). Submarine venting of phase-separated hydrothermal fluids at axial volcano, Juan de Fuca Ridge. *Nature*, *340*(6236), 702–705.

MBARI Mapping Team. (2001). *MBARI West Coast Seamounts and Ridges Multibeam Survey*. Moss Landing, CA: MBARI.

Metz, S., & Trefry, J. H. (2000). Chemical and mineralogical influences on concentrations of trace metals in hydrothermal fluids. *Geochimica et Cosmochimica Acta*, *64*(13), 2267–2279.

Michael, P. J., & Cornell, W. C. (1998). Influence of spreading rate and magma supply on crystallization and assimilation beneath mid-ocean ridges: Evidence from chlorine and major element chemistry of mid-ocean ridge basalts. *Journal of Geophysical Research: Solid Earth*, *103*(B8), 18325–18356.

Morton, J. L., Sleep, N. H., Normark, W. R., & Tompkins, D. H. (1987). Structure of the southern Juan de Fuca Ridge from seismic reflection records. *Journal of Geophysical Research: Solid Earth*, *92*(B11), 11315–11326.

Mottl, M. J. (2012). VentDB: mid-ocean ridge hydrothermal vent chemistry data collection in the EarthChem library. *Integrated Earth Data Applications (IEDA)*. https://doi.org/10.1594/IEDA/100207

Mullineaux, L. S., Metaxas, A., Beaulieu, S. E., Bright, M., Gollner, S., Grupe, B. M., et al. (2018). Exploring the ecology of deep-sea hydrothermal vents in a metacommunity framework. *Frontiers in Marine Science*, *5*, 49. https://doi.org/10.3389/fmars.2018.00049

Nehlig, P. (1991). Salinity of oceanic hydrothermal fluids: A fluid inclusion study. *Earth and Planetary Science Letters*, *102*(3–4), 310–325.

Normark, W. R., Morton, J. L., Bischoff, J. L., Brett, R., Holcomb, R. T., Kappel, E. S., et al. (1986). Submarine fissure eruptions and hydrothermal vents on the southern Juan de Fuca Ridge: Preliminary observations from the submersible Alvin: US Geological Survey Juan de Fuca Study Group. *Geology*, *14*(10), 823–827.

Normark, W. R., Morton, J. L., Koski, R. A., Clague, D. A., & Delaney, J. R. (1983). Active hydrothermal vents and sulfide deposits on the southern Juan de Fuca Ridge. *Geology*, *11*(3), 158–163.

Normark, W. R., Morton, J. L., & Ross, S. L. (1987). Submersible observations along the southern Juan de Fuca Ridge: 1984 Alvin program. *Journal of Geophysical Research: Solid Earth*, *92*(B11), 11283–11290.

Paduan, J. B., Zierenberg, R. A., Clague, D. A., Spelz, R. M., Caress, D. W., Troni, G., et al. (2018). Discovery of hydrothermal vent fields on Alarcón Rise and in Southern Pescadero Basin, Gulf of California. *Geochemistry, Geophysics, Geosystems*, *19*(12), 4788–4819. https://doi.org/10.1029/2018GC007771

Pester, N. J., Ding, K., & Seyfried, W. E., Jr. (2014). Magmatic eruptions and iron volatility in deep-sea hydrothermal fluids. *Geology*, *42*(3), 255–258. https://doi.org/10.1130/G35079.1

Pester, N. J., Ding, K., & Seyfried, W. E., Jr. (2015). Vapor–liquid partitioning of alkaline earth and transition metals in NaCl-dominated hydrothermal fluids: An experimental study from 360 to 465 C, near-critical to halite saturated conditions. *Geochimica et Cosmochimica Acta*, *168*, 111–132. https://doi.org/10.1016/j.gca.2015.07.028

Pester, N. J., Rough, M., Ding, K., & Seyfried, W. E., Jr. (2011). A new Fe/Mn geothermometer for hydrothermal systems: Implications for high-salinity fluids at 13 N on the East Pacific Rise. *Geochimica et Cosmochimica Acta*, *75*(24), 7881–7892. https://doi.org/10.1016/j.gca.2011.08.043

Scheirer, D. S., Fornari, D. J., Humphris, S. E., & Lerner, S. (2000). High-resolution seafloor mapping using the DSL-120 sonar system: Quantitative assessment of sidescan and phase-bathymetry data from the Lucky Strike segment of the Mid-Atlantic Ridge. *Marine Geophysical Researches*, *21*(1–2), 121–142.

Scheuermann, P. P., Tan, C., & Seyfried, W. E., Jr. (2018). Quartz solubility in the two-phase region of the NaCl-H2O system: An experimental study with Application to the Piccard hydrothermal field, mid-Cayman Rise. *Geochemistry, Geophysics, Geosystems*, *19*(9), 3570–3582. https://doi.org/10.1029/2018GC007610

Schoofs, S., & Hansen, U. (2000). Depletion of a brine layer at the base of ridge-crest hydrothermal systems. *Earth and Planetary Science Letters*, *180*(3–4), 341–353.

Scott, S., Driesner, T., & Weis, P. (2016). The thermal structure and temporal evolution of high-enthalpy geothermal systems. *Geothermics*, *62*, 33–47. https://doi.org/10.1016/j.geothermics.2016.02.004

Seewald, J. S., Cruse, A., & Saccocia, P. J. (2003). Aqueous volatiles in hydrothermal fluids from the Main Endeavour field, northern Juan de Fuca ridge: Temporal variability following earthquake activity. *Earth and Planetary Science Letters*, *216*, 575–590. https://doi.org/10.1016/S0012-821X(03)00543-0

Seewald, J. S., & Seyfried, W. E., Jr. (1990). The effect of temperature on metal mobility in subseafloor hydrothermal systems: Constraints from basalt alteration experiments. *Earth and Planetary Science Letters*, *101*(2–4), 388–403.

Seyfried, W. E., Jr., & Mottl, M. J. (1982). Hydrothermal alteration of basalt by seawater under seawater-dominated conditions. *Geochimica et Cosmochimica Acta*, *46*(6), 985–1002.

Seyfried, W. E., Jr., Seewald, J. S., Berndt, M. E., Ding, K., & Foustoukos, D. I. (2003). Chemistry of hydrothermal vent fluids from the Main Endeavour Field, northern Juan de Fuca Ridge: Geochemical controls in the aftermath of June 1999 seismic events. *Journal of Geophysical Research: Solid Earth*, *108*(B9).

Stakes, D. S., Chadwick, W. W., Jr., Maher, N., & Scheirer, D. S. (1998). Results of nested high-resolution mapping of the southern Cleft segment, Juan de Fuca Ridge. *Eos Transactions American Geophysical Union*, *79*(45, Fall Meeting Supplement), F810.

Trefry, J. H., Butterfield, D. B., Metz, S., Massoth, G. J., Trocine, R. P., & Feely, R. A. (1994). Trace metals in hydrothermal solutions from Cleft segment on the southern Juan de Fuca Ridge. *Journal of Geophysical Research: Solid Earth*, *99*(B3), 4925–4935.

Von Damm, K. L. (2004). Evolution of the hydrothermal system at East Pacific Rise 9° 50'N: Geochemical evidence for changes in the upper oceanic crust. In C. R. German, J. Lin, & L. M. Parson (Eds.), *Hydrothermal Interactions between the Lithosphere and Oceans, Geophysical Monograph Series* (Vol. 148, pp. 285–305). Washington, DC: American Geophysical Union.

Von Damm, K. L., & Bischoff, J. L. (1987). Chemistry of hydrothermal solutions from the southern Juan de Fuca Ridge. *Journal of Geophysical Research: Solid Earth*, *92*(B11), 11334–11346.

Von Damm, K. L., Bischoff, J. L., & Rosenbauer, R. J. (1991). Quartz solubility in hydrothermal seawater; an experimental study and equation describing quartz solubility for up to 0.5 M NaCl solutions. *American Journal of Science*, *291*(10), 977–1007.

Von Damm, K. L., Edmond, J. M., Grant, B., Measures, C. I., Walden, B., & Weiss, R. F. (1985). Chemistry of submarine hydrothermal solutions at 21° N, East Pacific Rise. *Geochimica et Cosmochimica Acta*, *49*(11), 2197–2220.

Von Damm, K. L., Lilley, M. D., Shanks Iii, W. C., Brockington, M., Bray, A. M., O'grady, K. M., et al. (2003). Extraordinary phase separation and segregation in vent fluids from the southern East Pacific Rise. *Earth and Planetary Science Letters*, *206*(3–4), 365–378. https://doi.org/10.1016/S0012-821X(02)01081-6

Wheat, C. G., Fisher, A. T., McManus, J., Hulme, S. M., & Orcutt, B. N. (2017). Cool seafloor hydrothermal springs reveal global geochemical fluxes. *Earth and Planetary Science Letters*, *476*, 179–188. https://doi.org/10.1016/j.epsl.2017.07.049

Xu, G., Chadwick, W. W., Jr., Wilcock, W. S., Bemis, K. G., & Delaney, J. (2018). Observation and modeling of hydrothermal response to the 2015 eruption at axial Seamount, Northeast Pacific. *Geochemistry, Geophysics, Geosystems*, *19*(8), 2780–2797. https://doi.org/10.1029/2018GC007607

Zierenberg, R., Friðleifsson, G. O., Elders, W., Schiffman, P., Fowler, A., Reed, M., et al. (2019). Alteration of sheeted dikes by supercritical seawater in an active hydrothermal system at Reykjanes, Iceland. Paper presented at the American Geophysical Union 2019 Fall Meeting. San Francisco, CA.